



Article

Design and Analysis of a Novel Adjustable SVAWT for Wind Energy Harvesting in New Energy Vehicle

Zhen Zhao ^{1,*}, Yongxin Li ¹, Baifu Zhang ², Changhong Wang ¹, Zhangwei Yan ¹ and Qingcheng Wang ¹

¹ School of Mechanical and Automobile Engineering, Liaocheng University, Liaocheng 252059, China

² College of Electrical and Power Engineering, Taiyuan University of Technology, Taiyuan 030024, China

* Correspondence: zhaozhennihao@126.com; Tel.: +0635-823-9211

Abstract: The new energy vehicle is a robust measure to solve the problem of global warming. However, the new energy vehicle generally has the disadvantages of short mileage and difficulty in finding public chargers. The combination of wind energy harvest and new energy vehicle can be conducive to the promotion of the new energy vehicle. This paper proposes a novel adjustable Savonius vertical axis wind turbine (SVAWT). It contains three parts: an energy absorption module, an energy recovery module, and an energy conversion module. The energy absorption module includes four blades with staggered distribution in two layers. The overlap ratio of the blades can be adjusted by the wind speed, which can ensure the SVAWT has a higher energy transfer efficiency. The energy recovery module adjusts the overlap ratio of the blades without interruption by utilizing the self-rotation and the orbital revolution of the gears. The energy conversion module converts mechanical energy into electric energy and supplies power for the vehicle after adjustment by the voltage regulator module. Based on actual operating data, it can be found that the variation trend of power of the blades absorbing is consistent with wind speed and increases with the wind speed. Under four actual operating conditions, the root mean square value of the blades absorbing power are 7.0 W, 7.1 W, 3.9 W, and 5.1 W, respectively. These results reveal that the proposed novel adjustable SVAWT has high recovery power potential and can provide a valuable solution to the practical applications of wind energy harvesting.



Citation: Zhao, Z.; Li, Y.; Zhang, B.; Wang, C.; Yan, Z.; Wang, Q. Design and Analysis of a Novel Adjustable SVAWT for Wind Energy Harvesting in New Energy Vehicle. *World Electr. Veh. J.* **2022**, *13*, 242. <https://doi.org/10.3390/wevj13120242>

Academic Editors: Yinghong Wu, Tiande Mo, Bo Li and Yang Luo

Received: 23 November 2022

Accepted: 13 December 2022

Published: 15 December 2022

Publisher's Note: MDPI stays neutral with regard to jurisdictional claims in published maps and institutional affiliations.



Copyright: © 2022 by the authors. Licensee MDPI, Basel, Switzerland. This article is an open access article distributed under the terms and conditions of the Creative Commons Attribution (CC BY) license (<https://creativecommons.org/licenses/by/4.0/>).

1. Introduction

Among the Sustainable Development Goals to be reached by 2030 [1], the United Nations posed an urgent call for action to reduce “the adverse per capita environmental impact of cities, including by paying particular to air quality.” In 2016, road transport accounted for 11.9% of global greenhouse gas emissions, 60% of which came from passenger travel [2,3]. In recent years, battery electric vehicles (BEVs) and plug-in hybrid electric vehicles (PHEVs), such as those from Tesla, BYD company limited, and some other vehicle manufacturers, have become increasingly popular to reduce the burden of fossil fuel consumption on the air. Some investigators have conducted surveys on the owners of BEVs and PHEVs. Based on the results from five-question surveys [4], discontinuing use occurs at a rate of 20% for PHEVs owners and 18% for BEVs owners.

The main reasons to abandon BEVs and PHEVs are short recharge mileage, slower charging speed, and difficulty finding public chargers [5–12]. In China, there is a serious distribution imbalance in public chargers. Public chargers have accounted for 46% of Beijing, Shanghai, Guangzhou, and Jiangsu, while the distribution of public chargers in other regions is limited. Currently, public chargers are used for an average of an hour a day in China, with a usage rate of 4%, while in Beijing, public chargers are used for 20 min a day, with a usage rate of only 1.3% [13].

Regarding environmental impact, thermal power generation accounts for 71.19% of China’s total power generation, according to the National Bureau of Statistics data of

China [14]. It will also cause substantial environmental pollution and cannot conform to the original intention of BEVs and PHEVs. Great River Energy [15], Minnesota's electric company, is committed to providing affordable, reliable, and cleaner energy. In 2020, 55% of the company's electric requirements were from thermal energy. They are transitioning from non-renewable energy and expect 57% of electricity to come from sustainable sources by 2027.

Therefore, how to extend the working time of PHEVs and BEVs by recycling energy is vitally important. In the current research on vehicle energy recovery [16–21], suspension vibration energy recovery, waste heat recovery, brake energy recovery, and renewable energy recovery are relatively common. Liwei Dong et al. [16] proposed a suspension vibration energy-regenerative shock absorber that adjusts damping by changing the external circuit to achieve maximum power recovery. Wei Yu et al. [17] proposed a refined energy management strategy considering suspension vibration energy recovery and waste heat recovery. The results showed that the proposed strategy's revenue increased with the recovered energy, thus improving the vehicle fuel economy.

For vehicles, renewable energy recovery contains solar energy recovery and wind energy recovery. Duan C et al. [18] proposed a solar energy harvesting-based modular battery balance system for EVs. Their experiments showed that the overall pure electric drive mileage can be increased by 22.9%, the total charging time can be reduced by 9.3%, and the power grid energy consumption may be decreased by 9.6%. Compared with solar energy recovery, wind energy has the advantage of high energy density and a comprehensive collection range. In conventional wind energy harvesting, a wind turbine can be divided into a Vertical Axis Wind Turbine (VAWT) and Horizontal Axis Wind Turbine (HAWT) according to the location difference of the rotation axis [22,23]. If the rotor axis is perpendicular to the ground, it is known as a VAWT. If the rotor axis is parallel to the ground, it is known as a HAWT. With its large sweep area and high wind energy utilization, the HAWT has gradually become the mainstream of wind turbines. Vahid Akbari et al. [24] chose 10 low Reynolds number airfoils, studied the power coefficient and the startup time of the HAWT by the blade element momentum technique, and performed a multi-objective optimization study in a 1kW wind turbine. Finally, a particular airfoil was selected to operate in windy regions and areas with low wind speeds. Similarly, Abdelgalil Eltayesh et al. [25] analyzed the influence of different blades and different tip speed ratios on a small-scale HAWT's power and thrust coefficients. Computational fluid dynamics (CFD) simulations and experimental measurements found that the HAWT with three-blade configurations had the maximum power coefficient compared with five and six blades, which is higher by around 2% and 4%, respectively.

Gideon Quartey et al. [19] proposed a wind turbine mounting on the vehicle's roof to generate electrical power to charge batteries when the vehicle is in motion. With the vehicle driving at 120 km/h, a huge amount of electrical power (about 3.26 kW) can be restored in the batteries by theoretical calculation. Awal et al. [20] investigated the installed structure of the wind turbine and proposed a novel installation method in which the generator is placed on the vehicle's roof and coupled with the turbine shaft by a belt. The installed method can increase the power of generation significantly. However, with the application of the HAWT, many faults have been exposed. When the HAWT is working, the blades cutting airflows produce a lot of noise, threatening birds' safety and polluting the surrounding environment [26,27]. Otherwise, the HAWT can only absorb the wind from some directions. If the direction of the wind is parallel with the blade plane, then the HAWT cannot operate, as it is limited by the installation place.

Compared with the HAWT, the VAWT overcomes these challenges. The VAWT contains two types: Savonius and Darrieus, based on the blade's pressure difference [28,29]. The Savonius-type turbine has many advantages over the Darrieus [30], such as structure simplicity, low-speed wind self-start, operation capabilities, good animal vision, the ability to catch wind from all directions, and a noiseless low-frequency noise. Due to these advantages, the Savonius Vertical Axis Wind Turbine (SVAWT) has been utilized in many

urban places to harvest wind energy [31–34]. However, through use, there is no doubt that the SVAWT cannot produce as much energy as other wind turbines, making it less powerful [29].

With the help of the finite volume solver ANSYS (ANSYS is a large, general purpose finite element analysis software developed by ANSYS, USA), Nur Alom et al. [23] analyzed the total pressure, velocity magnitude, and turbulence intensity of the SVAWT blade using the Shear Stress Transport k-w turbulence model. From the simulation results, the maximum power coefficients for the elliptical profiles of the blade can reach 0.34. Based on the conventional SVAWT, M.H. Paranta et al. [29] proposed a modified SVAWT. The proposed model performed better than the conventional model when $TSR = 1.1$, which is 62.5% higher than the traditional design. To increase the robustness of SVAWT, Sebastian Torres et al. studied a new design method for SVAWT to maximize its aerodynamic performance [35]. By defining a numerical model for geometry with four influencing parameters, the motion of fluids for different turbines can be calculated automatically.

Then, based on the Kriging technique, 340 different SVAWTs were built on a response surface with high-quality metrics. We can find the best parameter configuration through mathematical methods of the optimization algorithm. With the comprehension of the optimization algorithm, we can use a genetic algorithm to find the optimal parameter configuration [36]. After investigating many designs, the optimization result is considered the optimal global solution. Hassan Fathabadi et al. [21] appraised the possibility of utilizing a wind turbine to recapture a portion of the kinetic energy losses of a car. They inserted a small wind turbine at the back of the vehicle's condenser to avoid increasing the vehicle driving resistance. Experimental measurements conducted under realistic operation of the EV have been given that prove that the traveling range of the EV and the power efficiency of the EV's power supply are enhanced by, respectively, 6.4 km and 0.2% by recovering only a portion of the kinetic energy losses of the EV. These benefits prove the novelty and contributions of the work in successfully recovering a portion of the kinetic energy losses of a car using a small wind turbine embedded in the car. SOFIAN M et al. [37] gave essential insights into the advantages of a wind turbine installed in the front of a car. Sedan-type cars were modeled using the simulation performed by ANSYS FLUENT software. Three car models with different wind turbine system positions and one model without the wind turbine system were simulated. The simulation results showed that the wind turbine mounted in front of the car did not significantly affect the car's aerodynamic performance. The front of the car model seems to be a suitable area to install a wind turbine system. Chaudhary Y et al. [38] placed a set of two micro wind turbines along with two micro-generators on the rear end of the car trunk, evaluating the effect of drag force on the performance of the car through the experimental approach and CFD simulations. Both methods confirmed the negligible effect of drag force on the vehicle performance in terms of gas mileage and changes in drag coefficient values.

However, these studies have ignored some vital issues. The wind speed is not invariable, and the weather may be worse. M.S. Abdullah et al. [39] predicted the flow structure and the force response of various SVAWT diameters (D) from size 1D until 5D at different wind speeds (8–18 m/s) and bucket angles (0–180°) using the ANSYS Workbench environment 2019 R3. The static torque, blade deformation, stress-induced, and fatigue responses were studied extensively. The results showed that blade information increased proportionally with the turbine size and wind speed, shortening the service life of the SVAWT.

To sum up, it is essential to design a novel SVAWT that can be installed on the vehicle to extend the working time of BEVs and PHEVs and protect the device while improving the efficiency of wind energy recovery. In this paper, a novel adjustable SVAWT was designed and installed in the vehicle's front portion, near the vehicle's front grille. According to different vehicle speeds and weather, the motor can adjust the overlap ratio of the blades to improve the efficiency of the SVAWT and protect the device. A generator was used

to convert the rotary kinetic energy of the blades into electric energy and supply for the vehicle.

The rest of this paper is organized as follows. Section 2 describes the components and working principles of the SVAWT. The modeling and analysis of the SVAWT is given in Section 3. In Section 4, the simulation results under different conditions are discussed. Section 5 presents the conclusion and directions for future studies.

2. System Design

In vehicle driving, the air pressure around the vehicle will change. As we know, air always flows from high pressure to low pressure, which produces wind. The design of the vehicle's front grille promises a flow of wind into the vehicle's front portion, which can cool the engine while driving. This research work proposed a novel adjustable SVAWT to harvest this wind energy and designed it using the SOLIDWORKS 2020 software.

As shown in Figure 1, the design of the novel adjustable SVAWT proposed in this paper is mainly composed of three parts: an energy absorption module, an energy recovery module, and an energy conversion module. The SVAWT is installed in the front portion of the vehicle, near the vehicle's front grille. When the wind speed matches with the blades opening, the generator and the motor are in operation. When the wind speed does not correspond with the blades opening, the generator is in operation and the motor is not in operation. The mechanical energy converts into electrical energy. The electrical power is rectified and stored in the supercapacitor, providing energy for the lower-power sensors.

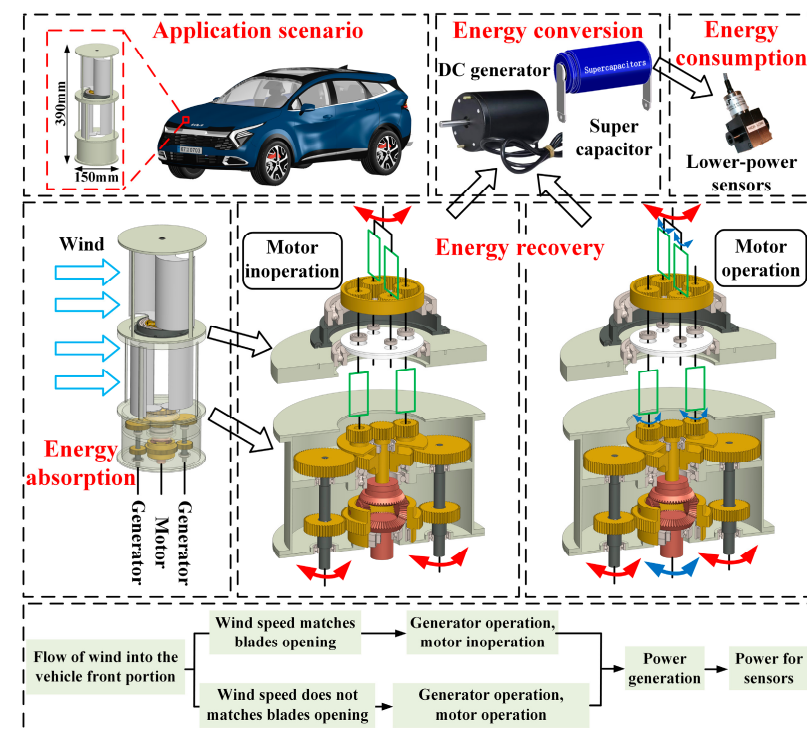


Figure 1. Flowchart of energy conversion using the novel adjustable SVAWT.

2.1. Energy Absorption Module

To eliminate the influence of the axial diameter on the fan, the SVWAT blade designed in this paper is a wind turbine without a central rotating shaft, as shown in Figure 2a. The concave part filled with wind absorbs air and induces the rotor blade to rotate, while the convex portion meets the air and drains the rotating shaft laterally. When moving to the wind, the curvature of the blade has lower resistance than the other blades. Therefore, the concave blade drives the rotor with a large drag force.

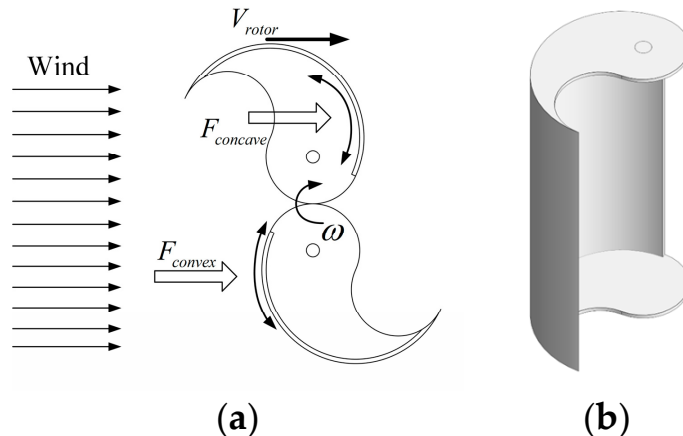


Figure 2. Blades of the energy absorption module. (a) Two blades with drag forces in the proposed SVAWT. (b) Shape of the blade.

The blade section is semi-circular, and the shape of the blade end fixed plate is similar to the ‘Eight Diagrams,’ as shown in Figure 2b. This design enables the two blades in the rotor to be closed (after the two blades are closed, they are combined into a whole cylindrical surface, and the two ends are combined into a circular surface), thereby making the rotor a closed cylinder, ensuring SVAWT Safety under harsh conditions (i.e., vehicles often drive in stormy weather).

Researchers have performed extensive work on the optimization of blades, such as CFD simulation optimization, structural optimization algorithm optimization, etc. The overlap ratio of the blades, which has been studied on the VAWT, always remains the same in the working process. The critical question of whether the vehicle speed and the weather cannot be set according to the experimental requirements has been dismissed. As shown in Figure 2a, in the process of working, the overlap ratio of the blades can be adjusted by the motor, which ensures that the blades can be matched with the vehicle speed and environment, improving energy recovery efficiency while protecting the device.

The advantages of the SVWAT designed in this paper are as follows: (1) The SVWAT has a low starting wind speed. (2) The blade is easy to manufacture and low-cost. The generator transmission mechanism and control mechanism are easy to repair. (3) The SVWAT has low noise.

2.2. Energy Recovery Module

As shown in Figure 3a, the energy recovery module mainly contains blades, gears 1–6, ring gear, bevel gears 1–3, and the shaft. The shaft connects with the generator, and the bevel gear 3 attaches to the motor. Reference [40] showed that the multi-stage rotor’s static and dynamic torque changes in a rotation cycle are considerably smooth compared with the ordinary one-stage rotor by wind tunnel test. To solve the contradiction between the high-power coefficient and the poor starting performance of the two-blade SVWT, combined with the limitation of vehicle installation space, this paper chose a two-blade, two-stage structure SVWT. Two one-stage SVWTs connected in the axial direction and series. There was a 90° phase difference between the two group blades above the ring gear and those below the ring gear.

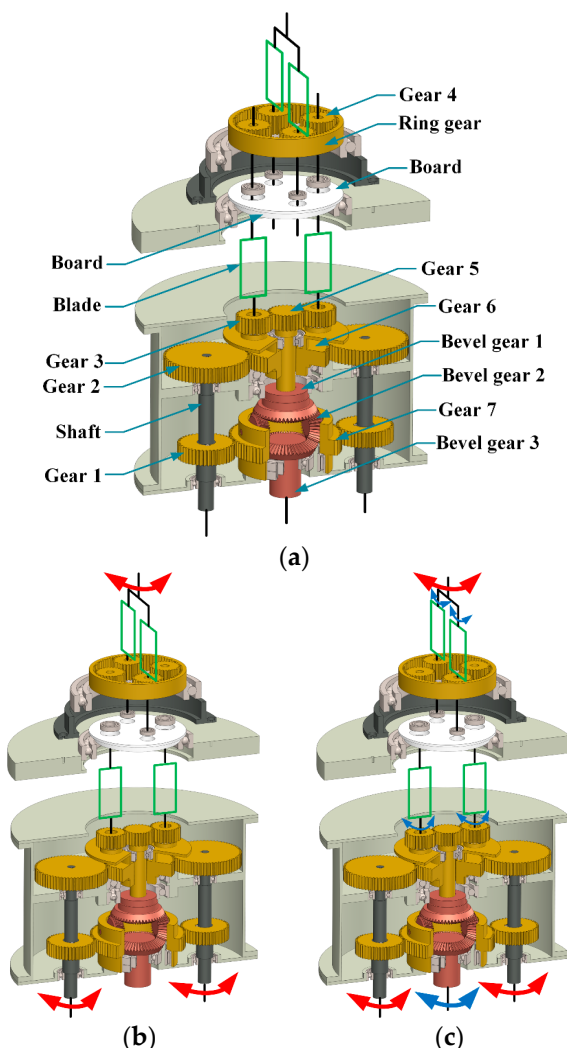


Figure 3. Energy recovery principle of the SVAWT. (a) Installation position of the novel adjustable SVAWT. (b) Motion transmission of the novel adjustable SVAWT when the motor is not in operation. (c) Motion transmission of the novel adjustable SVAWT when the motor is in operation.

2.2.1. Inoperative Motor

The blades are fixed with the gear by the key and convert the wind energy into mechanical energy. When the rotor overlap ratio matches with the vehicle speed and the weather, the motor is inoperative. As a result of bevel gear 3 being connected to the motor and the motor having ample starting torque if the motor is not working, the overlap ratio remains the same. Table 1 shows the parameters of the gear and bevel gear. As shown in Figure 3b, under the wind function, gear 6 produces rotation, assuming a rotational speed of n . Then, the rotational speed of gear 1 is n , the rotational speed of gear 7 is $n/2$, the rotational speed of the bevel gear 1 is n , and the rotational speed of gear 5 is n . So, gear 3 follows gear 5 for the orbital revolution.

Table 1. Parameters of the gears and bevel gears.

Parameters	Tooth Number	Parameters	Tooth Number
gear 1	44	gear 6	67
gear 2	67	gear 7	88
gear 3	27	bevel gear 1	51
gear 4	27	bevel gear 2	29
gear 5	27	bevel gear 3	51

2.2.2. Motor Operation

When the overlap ratio of the blades does not match the vehicle speed and the weather, the motor must work on promising the total energy transfer efficiency and the device's safety. As shown in Figure 4, when the overlap ratio needs to become more significant (from left to right), the motor drives bevel gear 3 to rotate. Assuming the rotational speed of gear 6 is n , the rotational speed of gear 5 is ($N > n$). Therefore, gear 5 and 6 will rotate relative to each other, and gear 3 will self-rotate during the orbital revolution with gear 6. The overlap ratio will change. The two blades above the ring gear and the two below the ring gear will have the same N overlap ratio. In Figure 3c, it is worth emphasizing that the shaft constantly rotates, and the generator works without interruption while the motor is operating (the overlap ratio is changing), decreasing the loss of the inertia energy.

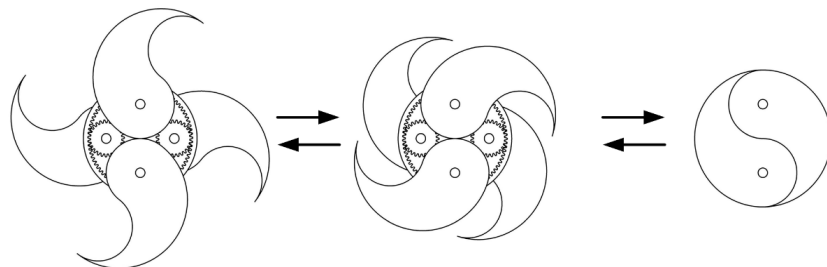


Figure 4. Various positions of the blades during motor operation.

2.3. Energy Conversion Module

The generator is connected with the shaft and converts mechanical energy into electrical energy according to the principle of electromagnetic induction. There are three kinds of generators options: (1) alternating current (AC) generators, (2) direct current (DC) generators, and (3) synchronous generators. AC generators are usually used in gasoline or diesel. They are suitable for large-scale power applications and not for wind energy recovery. When the synchronous generator runs at a high or low load, it is easy to generate vibration and heat, which can easily lead to a short circuit of the generator and shorten its service life. Consequently, the following DC generator was selected in this paper, as shown in Figure 5a. The main parameters of the DC generator are shown in Table 2. Because the rotation speed of the blades is changing, the voltage generated by the DC generator is in fluctuation. If the generator charges the supercapacitor with unstable voltage, it will give the supercapacitor a short service life. Therefore, the regulator module shown in Figure 5b was selected to regulate the generator output voltage. The input of the voltage regulator module is connected to the generator's output, and the production of the voltage regulator module is linked to the supercapacitor.

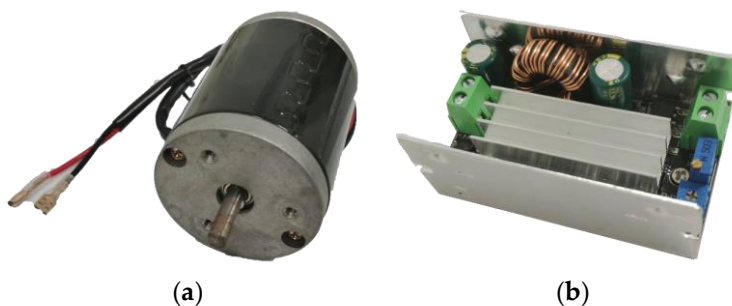


Figure 5. Components of the energy conversion module. (a) DC generator. (b) Voltage regulator module.

Table 2. Main parameters of the DC generator.

Parameters	Value
Diameter of input shaft	8 mm
Length	89 mm
Outer diameter	68 mm
Rated voltage	12 V
Rated speed	2000~4000 rpm
No-load current	0.2~3 A
Rated power	100 W
Rotor inertia	0.436 kg·cm ²

3. Modeling and Analysis

3.1. Rotor Model

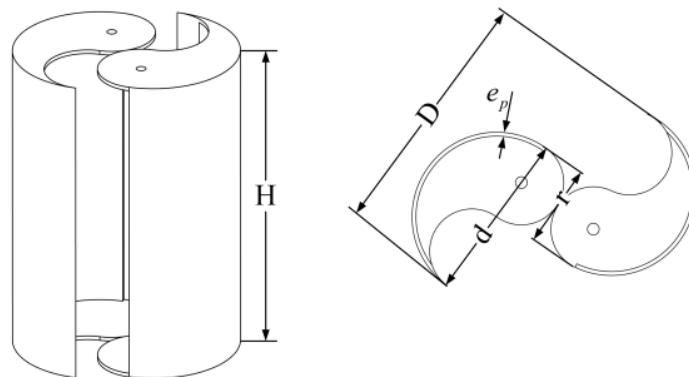
In Figure 6, H is the height of the blades, d is the diameter of a blade, e_p is the thickness of the blade, r is the eccentric distance, and D is the SVAWT diameter. Due to the blades being directly touched with the wind flow and absorbing the wind energy, modeling the blades is vitally important.

$$E_w = mv^2/2 \quad (1)$$

$$m = \rho A(t) \cdot v(t) \quad (2)$$

where ρ is the density of the air, A is the area sweeping by the blades, $A = D \times H$, v is the speed of the wind (wind speed is approximately equal to the vehicle speed), m is the wind mass of the area sweeping, and E_w (wind energy) is the kinetic energy of the air sweeping by the blades per second [41]. Combining Equation (2) with Equation (1), the power of the area sweeping can be calculated:

$$E_w = \rho A(t) \cdot v^3(t)/2 \quad (3)$$

**Figure 6.** Main shape parameters of the blades of the novel adjustable SVAWT.

The wind speed cannot decrease to zero after the wind passes through the blades. In other words, the air sweeping by the blades cannot transmit all the energy to the blades. Hence, the blades can only receive part of the energy of the wind.

$$c_p = \frac{P}{E_w} = \frac{2P}{\rho A(t) \cdot v^3(t)} \quad (4)$$

where P is the power acquired by the blades and c_p is the wind turbine airfoils.

According to Betz's Law, the maximum value of the wind turbine airfoils is 0.593. However, the SVAWT is limited to many factors, such as its installation position and structure damping. Therefore, the normal value of the wind turbine airfoils ranges from 0.4

to 0.45 in practice. So, we set the value of the wind turbine airfoils of the novel adjustable SVAWT as 0.4.

Blades absorb wind energy and are mainly used in two parts: As part of the energy to make components rotate (E_T), such as gear rotation, blade rotation, and generator rotor rotation. Another part of the energy is used to neutralize the overlapping damping force (E_C), such as the meshing damping force between gears, the electrical damping force of the generator, etc.

3.1.1. Rotational Energy of Components

Using the energy method, the energy of the rotation of the components could be obtained as follows [42]:

$$\begin{aligned} E_T = & \frac{1}{2}J_r\omega_r^2 + 6 \times \frac{1}{2}J_{g4}\omega_{g4}^2 + \frac{1}{2}J_b\omega_b^2 + 4 \times \frac{1}{2}J_s\omega_s^2 + 2 \times \frac{1}{2}J_{ge}\omega_{ge}^2 \\ & + \frac{1}{2}J_{g5}\omega_{g5}^2 + \frac{1}{2}J_{g6}\omega_{g6}^2 + 2 \times \frac{1}{2}J_{g2}\omega_{g2}^2 + 2 \times \frac{1}{2}J_t\omega_t^2 \\ & + 2 \times \frac{1}{2}J_{g1}\omega_{g1}^2 + \frac{1}{2}J_{g7}\omega_{g7}^2 + \frac{1}{2}J_{bg1}\omega_{bg1}^2 + 2 \times \frac{1}{2}J_{bg2}\omega_{bg2}^2 \end{aligned} \quad (5)$$

where J_r and ω_r are the rotary inertia and angular velocity of the ring gear, J_{g4} and ω_{g4} are the rotary inertia and angular velocity of the gear 4, J_b and ω_b are the rotary inertia and angular velocity of the board, J_s and ω_s are the rotary inertia and angular velocity of the blade, J_{ge} and ω_{ge} are the rotary inertia and angular velocity of the rotor of the DC generator, J_{g5} and ω_{g5} are the rotary inertia and angular velocity of the gear 5, J_{g6} and ω_{g6} are the rotary inertia and angular velocity of the gear 6, J_{g2} and ω_{g2} are the rotary inertia and angular velocity of the gear 2, J_t and ω_t are the rotary inertia and angular velocity of the shaft, J_{g1} and ω_{g1} are the rotary inertia and angular velocity of the gear 1, J_{g7} and ω_{g7} are the rotary inertia and angular velocity of the gear 7, J_{bg1} and ω_{bg1} are the rotary inertia and angular velocity of the bevel gear 1, and J_{bg2} and ω_{bg2} are the rotary inertia and angular velocity of the bevel gear 2.

3.1.2. Energy of Overlapping Damping Force of the Novel Adjustable SVAWT

The mesh damping between gears 1 and 2 can be obtained from [42].

$$C_k = 2\xi \sqrt{\frac{k_g r_1 r_2 J_1 J_2}{r_1^2 J_1 + r_2^2 J_2}} \quad (6)$$

where ξ is the damping ratio which ranges from 0.03 to 0.17, with 0.1 taken as its value herein; k_g is the mean value of the stiffness in the corresponding mesh pair 1 and 2; r_1 and r_2 are the radius of the mesh gears 1 and 2; and J_1 and J_2 are the rotary inertia of the mesh gears 1 and 2.

In [43], the dynamics and the electrical damping characteristics of the DC generator were analyzed. By ignoring the inductance, the resistive torque T_{ge} induced by the electrical damping of the DC generator can be expressed as [44]:

$$T_{ge} = \frac{3k_t k_e}{2(R_i + R_e)} \omega_{ge} = C_{ge} \omega_{ge} \quad (7)$$

where k_t is the speed constants, k_e is the torque constants, R_i is the internal resistance of the generator, R_e is the external resistance of the generator, C_{ge} is the electromagnetic damping of the generator, and ω_{ge} is the angular velocity of the generator.

Hence, the power of the overlapping damping force can be calculated:

$$P_M = 2C_1\omega_{g2}^2 + 2C_2\omega_{g1}^2 + 2C_3\omega_{bg1}^2 + 2C_4\omega_{bg3}^2 + 2C_{ge}\omega_{ge}^2 \quad (8)$$

where C_1 is the mesh damping between gears 2 and 6, C_2 is the mesh damping between gears 1 and 7, C_3 is the mesh damping between bevel gears 1 and 2, C_4 is the mesh damping

between bevel gears 2 and 3, and ω_{bg3} is the angular velocity of the bevel gears 3 (as the angular velocity of the motor).

Then, the energy of the overlapping the damping force can be calculated:

$$E_C = \int P_M dt \quad (9)$$

3.2. Generator Model

The generator used herein is a DC generator. According to Newton's second law, the equation of motion of the generator can be expressed as:

$$T_m - T_{ge} = J_{ge}\dot{\omega}_{ge} \quad (10)$$

where T_m is the input torque of the generator.

The power generated by the DC generator can be obtained as follows:

$$P_D = 2(T_m - T_{ge})\omega_{ge} = 2J_{ge}\dot{\omega}_{ge}\omega_{ge} \quad (11)$$

3.3. Efficiency Analysis of the Novel Adjustable SVAWT

The wind flow receives the resistance force of the blades after entering the front of the vehicle. Due to the different pressures on both sides of the blade, the blade converts wind energy into mechanical energy. When the coincidence degree of the blade does not match the speed and weather, the motor starts to work. Under the action of the motor, gears 4, 3, and bevel gear 2 rotate. In this paper, we ignored the energy consumption of the motor during operation, so the total energy transfer efficiency of the device can be expressed as:

$$\eta = \frac{4J_{ge}\dot{\omega}_{ge}\omega_{ge}}{\rho A(t) \cdot v^3(t)} \quad (12)$$

4. Results and Discussion

With the above modeling and analysis section, we selected a new energy electric vehicle as the research object. The energy recovery effect of the novel adjustable SVAWT installed on the vehicle was analyzed by MATLAB software and based on the four sets of actual operating condition data when driving in an urban area. Figure 7 shows the vehicle speed curves under the four operating conditions. We carried out four groups of tests in urban areas, and the speed was mainly concentrated in the range of 10~12 m/s; at the same time, affected by Traffic Signal Lights, vehicles often accelerated and decelerated and had parking phenomenon. The novel adjustable SVAWT was mounted in the front of the vehicle, adjacent to the front grille. Combined with the reference's conclusion and the research object of this paper, it can be concluded that when SVAWT is installed in the front of the vehicle adjacent to the front grille, the drag coefficient does not change compared with that without the SVAWT system [37,38]. So, there is a negligible effect of drag force on the vehicle performance in terms of gas mileage and changes in drag coefficient values. That is, the total resistance energy of the car and the turbine does not exceed the resistance energy of the car without the SVAWT system. The wind speed and vehicle speed are relative because most of the vehicle is subject to frontal wind, so the vehicle's speed can be approximated as the wind speed [45]. In this paper, to recover more wind power, the overlap ratio can be adjusted according to the driving speed, thereby improving the energy utilization rate of the vehicle.

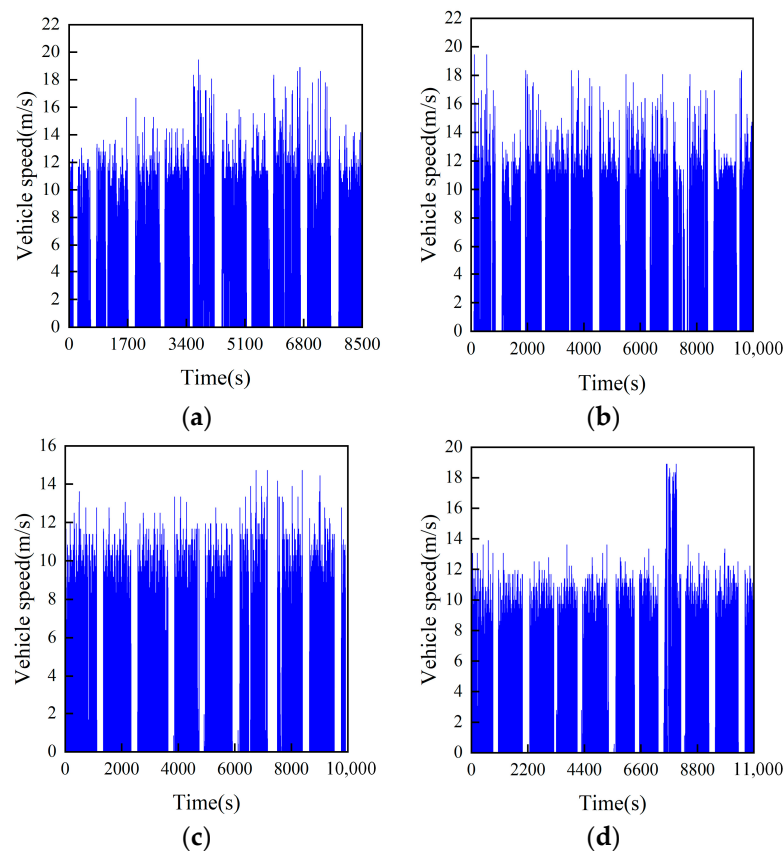


Figure 7. Variation curve of vehicle speed. (a) Operating condition 1. (b) Operating condition 2. (c) Operating condition 3. (d) Operating condition 4.

The blades rotate after the action of the wind, transferring the wind energy into the mechanical energy of the blades. The overlap ratio and the diameters of the blades are changeable at different wind speeds. The variation curve of the blade diameter with the wind speed is shown in Figure 8. When the speed sensor measured the wind speed (vehicle speed) between 0 m/s and 12 m/s, the motor was not in operation, and the diameter of the blades was unchangeable, maintaining a size of 120 mm. When the wind speed was between 12 m/s and 20 m/s, the motor was in operation, and the diameter of the blades decreased in proportion from 120 mm to 60 mm. When the wind speed surpassed 20 m/s, the motor was not in operation, and the blades' diameter was never changeable, maintaining a size of 60mm, which protected the blades from the heavy wind speed. Then, according to the Equations (3) and (4), the power of the blades can be obtained. Figure 9 shows the power of the blades absorbing the wind under four operating conditions.

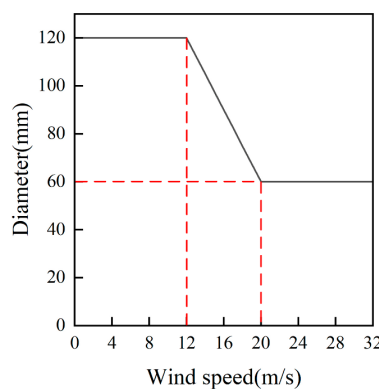


Figure 8. Relationship between the diameter of the blades and the wind speed.

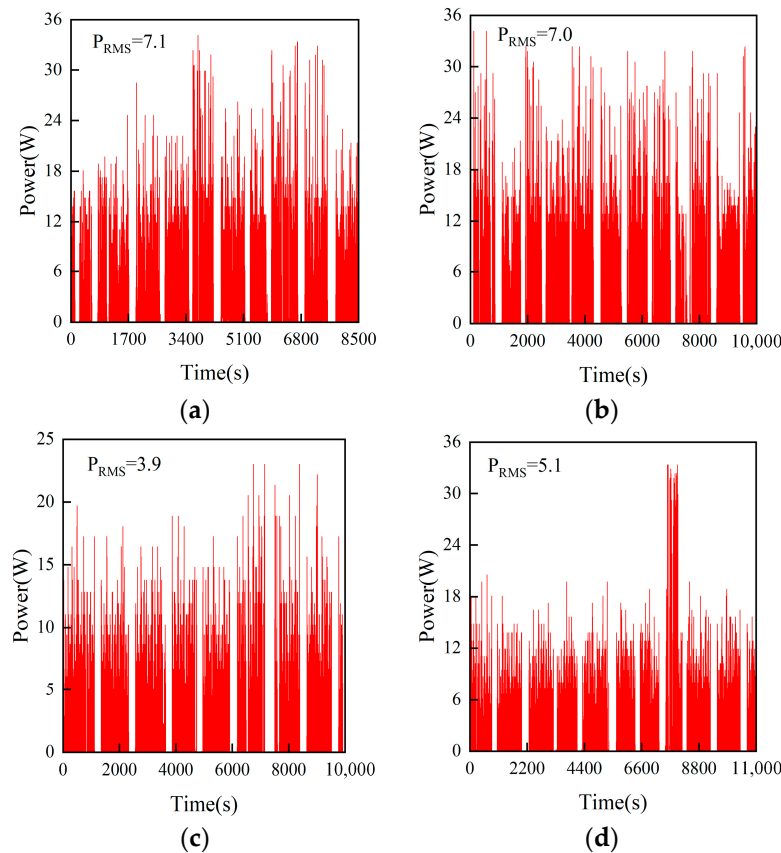


Figure 9. Power of the blades absorbing the wind under four operating conditions. (a) Power of the blades under operating condition 1. (b) Power of the blades under operating condition 2. (c) Power of the blades under operating condition 3. (d) Power of the blades under operating condition 4.

Comparing Figure 7 with Figure 9, it is found that the variation trend of power was consistent with that of wind speed and increased with the increase of wind speed. The root mean square (RMS) values of the power of the blades were 7.0 W, 7.1 W, 3.9 W, and 5.1 W under the four operating conditions. Then, combining Equation (5) and Equation (9), the angular velocity of the generator can be calculated, as shown in Figure 10.

By comparing Figures 7 and 10, it can be found that when the wind speed was zero, the angular velocity of the generator gradually decreased and then gradually increased. The reason for this phenomenon is that when the vehicle entered the parking state from the driving condition, the angular velocity of the generator decreased slowly under the action of the blade's inertia. When the vehicle entered the driving state from the parking state, the angular velocity of the motor also increased slowly under the action of the blade's inertia.

Compared with the previously proposed wind energy harvesting methods in vehicles [19,20], the advantages of the adjustable SVWAT designed in this paper are as follows: (1) The SVWAT has a low starting wind speed, small dimension, low noise, can be attached to space available, and is suitable for installation and use in new energy vehicles. (2) The blade is easy to manufacture and low cost. The generator transmission mechanism and control mechanism are easy to repair. (3) The overlap ratio of the blades can be adjusted by the wind speed, which can ensure the SVAWT has a higher energy transfer efficiency. The main disadvantage of the adjustable SVWAT is that the power is relatively small. The main reason for this phenomenon is that the device has lower wind energy recovery efficiency than the horizontal axis power generation device, a small overall size, and a low test speed. In summary, the proposed novel adjustable SVAWT has higher stability, energy conversion efficiency, adaptability, electrical performance, and service life under the simulation of the

actual training operation, providing an essential reference for harvesting wind energy to charge the battery.

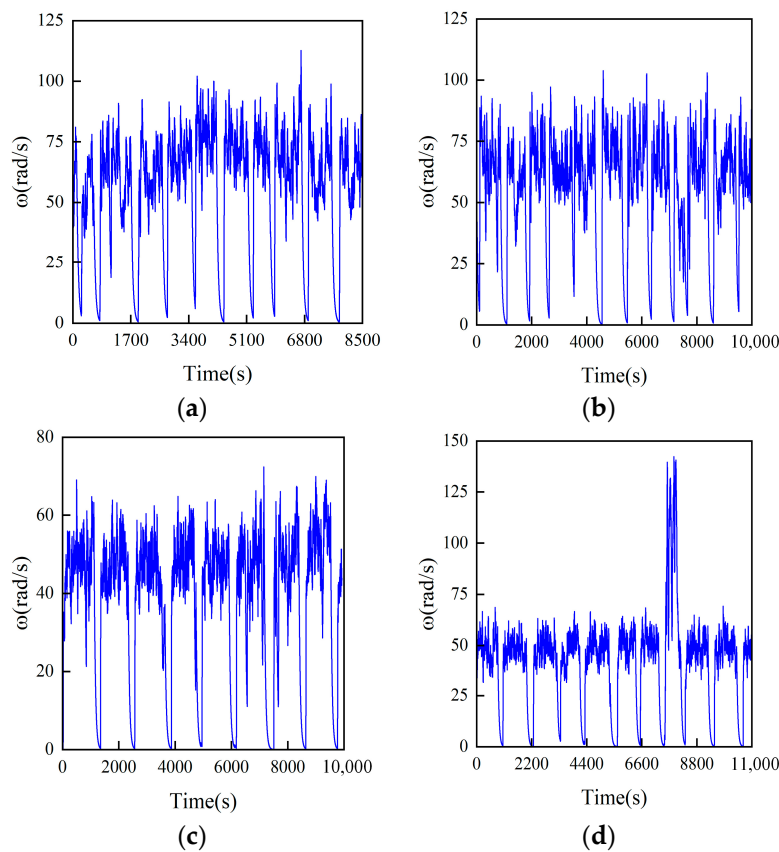


Figure 10. Angular velocity of the generator under four operating conditions. (a) Angular velocity under operating condition 1. (b) Power of the blades under operating condition 2. (c) Power of the blades under operating condition 3. (d) Power of the blades under operating condition 4.

In the research, without increasing the vehicle's drag coefficient, the new adjustable SVAWT used air resistance to drive the blade rotation in the device to drive the generator to generate electricity. After conversion by a voltage regulator module, the EV's battery was charged or directly supplied some loads of EVs, thereby increasing the driving range.

5. Conclusions

In this paper, we designed a novel adjustable SVAWT for a vehicle, which converts wind energy into electric energy and can power supply low-power appliances on vehicles directly. The proposed SVAWT contains three parts: an energy absorption module, an energy recovery module, and an energy conversion module. The energy absorption module includes four blades, with staggered distribution in two layers. The overlap ratio of the blades can be adjusted by the wind speed and weather, which can ensure the SVAWT has a higher energy transfer efficiency. The energy recovery module ensures the generator works without interruption by utilizing the self-rotation and the orbital revolution of the gears. At the same time, the overlap ratio of the blades is adjusted. The energy conversion module converts mechanical energy into electric energy and supplies power for the vehicle after adjustment by the voltage regulator module. Based on the actual operating data, we analyzed the relationship between the wind speed, the blades' absorbing power, and the generator's angular velocity. The variation trend of power of the blades absorbing was consistent with wind speed and increased with the wind speed. Under the four operating conditions, the RMS values of the blades absorbing power were 7.0 W, 7.1 W, 3.9 W, and 5.1 W, respectively. These results reveal that the proposed novel adjustable

SVAWT has higher stability and broad wind speed range for the application. This work may provide a valuable and significant solution to the practical applications of wind energy harvesting. In future research, some lacking areas need to be fulfilled, such as making the prototype of the proposed module to prove the analysis results. The relationship between the blades' diameter and wind speed still needs many experiments to verify its correctness and rationality.

Author Contributions: Conceptualization, Z.Z. and Y.L.; methodology, Z.Z.; software, Y.L.; Writing—original draft, Z.Z. and Y.L.; Project administration and funding acquisition, Z.Z.; validation, B.Z., C.W., Z.Y., and Q.W. Writing—review and editing, Z.Z. and B.Z. All authors have read and agreed to the published version of the manuscript.

Funding: This research is supported by the Natural Science Fund Project of Shandong (ZR2020ME128, ZR2020ME113); Multi-objective Robust Design and Control of Multi-route Plug-in Hybrid Electric Bus (ZR2020ME128); Research on Coordinated Control Theory of Distributed Drive Electric Vehicle for Torque Inconsistency (ZR2020ME113).

Data Availability Statement: Not applicable.

Conflicts of Interest: The authors declare no conflict of interest.

Nomenclature

H	blade height	ρ	air density
d	blade diameter	A	blade area sweeping,
e_p	blade thickness	m	area sweeping wind mass
r	eccentric distance	v	wind speed
D	SVAWT diameter	E_w	blades kinetic energy
ξ	damping ratio	P	blades acquired power
k_g	pair 1 and 2 mesh stiffness	c_p	wind turbine airfoils
r_1	mesh gears 1 radius	r_2	mesh gears 2 radius
J_b	board rotary inertia	ω_b	board angular velocity
J_r	ring gear rotary inertia	ω_r	ring gear angular velocity
J_1	mesh gears 1 rotary inertia	J_2	mesh gears 2 rotary inertia
T_{ge}	resistive torque	C_{ge}	generator electromagnetic damping
k_t	speed constants	k_e	torque constants
R_i	generator internal resistance	R_e	generator external resistance
J_s	blade rotary inertia	ω_s	blade angular velocity
J_{ge}	DC generator rotary inertia	ω_{ge}	DC generator angular velocity
J_{bgi}	bevel gear i rotary inertia	ω_{bgi}	bevel gear i angular velocity
J_{gi}	gear i rotary inertia	ω_{gi}	gear i angular velocity
J_t	shaft rotary inertia	ω_t	shaft angular velocity
C_1	gears 2 and gears 6 mesh damping	C_3	bevel gears 1 and 2 mesh damping
C_2	gears 1 and gears 7 mesh damping	C_4	bevel gears 2 and 3 mesh damping
T_m	generator input torque	E_C	damping force energy
E_T	components rotate energy	η	energy transfer efficiency

Abbreviations

BEVs	battery electric vehicles	VAWT	vertical axis wind turbine
PHEVs	plug-in hybrid electric vehicles	HAWT	horizontal axis wind turbine
CFD	computational fluid dynamics	AC	alternating current
SVAWT	savonius vertical axis wind turbine	DC	direct current

References

- United Nations General Assembly Transforming Our World: The 2030 Agenda for Sustainable Development. Available online: <https://sdgs.un.org/2030agenda> (accessed on 23 November 2022).
- Edenhofer, O.; Pichs-Madruga, R.; Sokona, Y.; Minx, J.C. *Change 2014: Mitigation of Climate Change. Contribution of Working Group III to the Fifth Assessment Report of the Intergovernmental Panel on Climate Change*; Cambridge University Press: Cambridge, UK, 2014.
- Sector by Sector: Where do Global Greenhouse Gas Emissions Come from? *Our World in Data* n.d. Available online: <https://ourworldindata.org/ghg-emissions-by-sector> (accessed on 2 November 2022).
- Hardman, S.; Tal, G. Understanding discontinuance among California's electric vehicle owners. *Nat. Energy* **2021**, *6*, 538–545. [CrossRef]
- Rezvani, Z.; Jansson, J.; Bodin, J. Advances in consumer electric vehicle adoption research: A review and research agenda. *Transp. Res. Part D-Transp. Environ.* **2015**, *34*, 122–136. [CrossRef]
- Jabbari, P.; Chernicoff, W.; MacKenzie, D. Analysis of Electric Vehicle Purchaser Satisfaction and Rejection Reasons. *Transp. Res. Board* **2017**, *2628*, 110–119. [CrossRef]
- Adepetu, A.; Keshav, S. The relative importance of price and driving range on electric vehicle adoption: Los Angeles case study. *Transportation* **2017**, *44*, 353–373. [CrossRef]
- She, Z.-Y.; Sun, Q.; Ma, J.-J.; Xie, B.-C. What are the barriers to widespread adoption of battery electric vehicles? A survey of public perception in Tianjin, China. *Transp. Policy* **2017**, *56*, 29–40. [CrossRef]
- Vassileva, L.; Campillo, J. Adoption barriers for electric vehicles: Experiences from early adopters in Sweden. *Energy* **2017**, *120*, 632–641. [CrossRef]
- Franke, T.; Neumann, I.; Buehler, F.; Cocron, P.; Krems, J.F. Experiencing Range in an Electric Vehicle: Understanding Psychological Barriers. *Appl. Psychol.* **2012**, *61*, 368–391. [CrossRef]
- Dumortier, J.; Siddiki, S.; Carley, S.; Cisney, J.; Krause, R.M.; Lane, B.W.; Rupp, J.A.; Graham, J.D. Effects of providing total cost of ownership information on consumers' intent to purchase a hybrid or plug-in electric vehicle. *Transp. Res. Part A-Policy Pract.* **2015**, *72*, 71–86. [CrossRef]
- Does Driving Range of Electric Vehicles Influence Electric Vehicle Adoption? n.d. Available online: <https://ideas.repec.org/a/gam/justa/v9y2017i10p1783-d113883.html> (accessed on 2 November 2022).
- Zheng, P.; Fang, Z.; Li, H.; Pan, Y.; Luo, D.; Zhang, Z. Multi-objective optimization of hybrid energy management system for expressway chargers. *J. Energy Storage* **2022**, *54*, 105233. [CrossRef]
- Tan, C.; Geng, S.; Tan, Z.; Wang, G.; Pu, L.; Guo, X. Integrated energy system–Hydrogen natural gas hybrid energy storage system optimization model based on cooperative game under carbon neutrality. *J. Energy Storage* **2021**, *38*, 102539. [CrossRef]
- Electricity. Great River Energy n.d. Available online: <https://greatriverenergy.com/electricity-sources/> (accessed on 2 November 2022).
- Dong, L.; Yang, F.; He, A.; Guo, Z.; Yu, J.; Zuo, J. Investigation on energy-regenerative shock absorber with adjustable damping and power for freight wagons. *Energy Convers. Manag.* **2022**, *254*, 115228. [CrossRef]
- Yu, W.; Wang, R. Development and performance evaluation of a comprehensive automotive energy recovery system with a refined energy management strategy. *Energy* **2019**, *189*, 116365. [CrossRef]
- Duan, C.; Tao, H.; Wang, C.; Chen, J.; Zhao, X.; Zhou, X. An Electric Vehicle Battery Modular Balancing System Based on Solar Energy Harvesting. In Proceedings of the 2019 IEEE Transportation Electrification Conference and Expo (ITEC), Detroit, MI, USA, 19–21 June 2019.
- Quartey, G. Generation of Electrical Power by a Wind Turbine for Charging Moving Electric Cars. *J. Energy Technol. Policy* **2014**, *4*, 19–29.
- Awal, M.R.; Jusoh, M.; Sakib, M.D.; Hossain, F.; Rashidi, M.; Beson, C.; Aljunid, S.A. Design and implementation of Vehicle Mounted Wind Turbine. *ARPJ Eng. Appl. Sci.* **2015**, *10*, 8699–8706.
- Fathabadi, H. Possibility of Utilizing Wind Turbine to Recover a Portion of the Kinetic Energy Losses of a Car. *IEEE Trans. Veh. Technol.* **2019**, *68*, 8663–8670. [CrossRef]
- Battisti, L. *Relevance of Icing for Wind Turbines. Wind Turbines in Cold Climates*; Springer International Publishing: Cham, Switzerland, 2015; pp. 43–111. [CrossRef]
- Alom, N.; Saha, U.K. Influence of blade profiles on Savonius rotor performance: Numerical simulation and experimental validation. *Energy Convers. Manag.* **2019**, *186*, 267–277. [CrossRef]
- Akbari, V.; Naghashzadegan, M.; Kouhikamali, R.; Afsharpanah, F.; Yaici, W. Multi-Objective Optimization and Optimal Airfoil Blade Selection for a Small Horizontal-Axis Wind Turbine (HAWT) for Application in Regions with Various Wind Potential. *Machines* **2022**, *10*, 687. [CrossRef]
- Eltayesh, A.; Castellani, F.; Burlando, M.; Hanna, M.B.; Huzayyin, A.; El-Batsh, H.M.; Becchetti, M. Experimental and numerical investigation of the effect of blade number on the aerodynamic performance of a small-scale horizontal axis wind turbine. *Alex. Eng. J.* **2021**, *60*, 3931–3944. [CrossRef]
- Chaudhry, H.N.; Calautit, J.K.; Hughes, B.R. Computational Analysis to Factor Wind into the Design of an Architectural Environment. *Model. Simul. Eng.* **2015**, *2015*, e234601. [CrossRef]

27. Tjiu, W.; Marnoto, T.; Mat, S.; Ruslan, M.H.; Sopian, K. Darrieus vertical axis wind turbine for power generation II: Challenges in HAWT and the opportunity of multi-megawatt Darrieus VAWT development. *Renew. Energy* **2015**, *75*, 560–571. [CrossRef]
28. Aslam Bhutta, M.M.; Hayat, N.; Farooq, A.U.; Ali, Z.; Jamil, S.h.R.; Hussain, Z. Vertical axis wind turbine—A review of various configurations and design techniques. *Renew. Sustain. Energy Rev.* **2012**, *16*, 1926–1939. [CrossRef]
29. Pranta, M.H.; Rabbi, M.S.; Roshid, M.M. A computational study on the aerodynamic performance of modified savonius wind turbine. *Results Eng.* **2021**, *10*, 100237. [CrossRef]
30. Al-Faruk, A.; Sharifian, A. Geometrical optimization of a swirling Savonius wind turbine using an open jet wind tunnel. *Alex. Eng. J.* **2016**, *55*, 2055–2064. [CrossRef]
31. Ricci, R.; Vitali, D.; Montelpare, S. An innovative wind-solar hybrid street light: Development and early testing of a prototype. *Int. J. Low-Carbon Technol.* **2015**, *10*, 420–429. [CrossRef]
32. Ricci, R.; Romagnoli, R.; Montelpare, S.; Vitali, D. Experimental study on a Savonius wind rotor for street lighting systems. *Appl. Energy* **2016**, *161*, 143–152. [CrossRef]
33. Renewable Energy Resources | John Twidell, Tony Weir | Taylor & Francis n.d. Available online: <https://www.taylorfrancis.com/books/mono/10.4324/9781315766416/renewable-energy-resources-john-twidell-tony-weir> (accessed on 2 November 2022).
34. Alam, F.; Golde, S. An Aerodynamic Study of a Micro Scale Vertical Axis Wind Turbine. *Procedia Eng.* **2013**, *56*, 568–572. [CrossRef]
35. Torres, S.; Marulanda, A.; Montoya, M.F.; Hernandez, C. Geometric design optimization of a Savonius wind turbine. *Energy Convers. Manag.* **2022**, *262*, 115679. [CrossRef]
36. Marinić-Kragić, I.; Vučina, D.; Milas, Z. Global optimization of Savonius-type vertical axis wind turbine with multiple circular-arc blades using validated 3D CFD model. *Energy* **2022**, *241*, 122841. [CrossRef]
37. Sofian, M.; Nurhayati, R.; Rexca, A.J.; Syariful, S.S.; Aslam, A. An Evaluation of Drag Coefficient of Wind Turbine System Installed on Moving Car. *Appl. Mech. Mater.* **2014**, *660*, 689–693. [CrossRef]
38. Chaudhary, Y.; Bangi, V.; Guduru, R.; Aung, K.; Reddy, G. Preliminary Investigation on Generation of Electricity Using Micro Wind Turbines Placed on A Car. *Int. J. Renew. Energy Dev.* **2017**, *6*, 75–81. [CrossRef]
39. Abdullah, M.S.; Ishak, M.H.H.; Ismail, F. Numerical study of the 3D Savonius turbine under stationary conditions. *Eng. Fail. Anal.* **2022**, *136*, 106199. [CrossRef]
40. Wei, W.; Xu, J. Lateral and Longitudinal Overlap Ratio on Starting Performance of Savonius Wind Turbine. *Ind. Control. Comput.* **2017**, *30*, 52–54.
41. Morshed, K.N.; Rahman, M.; Molina, G.; Ahmed, M. Wind tunnel testing and numerical simulation on aerodynamic performance of a three-bladed Savonius wind turbine. *Int. J. Energy Environ. Eng.* **2013**, *4*, 18. [CrossRef]
42. Wang, H.; He, C.; Lv, S.; Sun, H. A new electromagnetic vibrational energy harvesting device for swaying cables. *Appl. Energy* **2018**, *228*, 2448–2461. [CrossRef]
43. Lin, T.; Pan, Y.; Chen, S.; Zuo, L. Modeling and field testing of an electromagnetic energy harvester for rail tracks with anchorless mounting. *Appl. Energy* **2018**, *213*, 219–226. [CrossRef]
44. Pan, Y.; Lin, T.; Qian, F.; Liu, C.; Yu, J.; Zuo, J.; Zuo, L. Modeling and field-test of a compact electromagnetic energy harvester for railroad transportation. *Appl. Energy* **2019**, *247*, 309–321. [CrossRef]
45. Hussain, M.Z.; Anbalagan, R.; Jayabalakrishnan, D.; Muruga, D.N.; Prabhahar, M.; Bhaskar, K.; Sendilvelan, S. Charging of car battery in electric vehicle by using wind energy. *Mater. Today Proc.* **2021**, *45*, 5873–5877. [CrossRef]